JOURNAL OF PROPULSION AND POWER
Vol. 14, No. 4, July–August 1998

Shock-Loss Model for Transonic and Supersonic Axial Compressors with Curved Blades

M. T. Schobeiri*
Texas A&M University, College Station, Texas 77843-3123

Reliable efficiency calculation of high-subsonic and transonic compressor stages requires a detailed and accurate prediction of the flowfield within these stages. Despite the tremendous progress in turbomachinery computational fluid mechanics, the compressor designer still uses different loss correlations to estimate the total pressure losses and thus the efficiency of the compressor stage. A new shock-loss model is presented for transonic and supersonic axial compressors with circular arc blade profiles. The model calculates the shock position, Mach number, expansion angle, and the shock total pressure losses. The model is integrated into a loss calculation procedure, where the shock, profile, secondary, and total losses are calculated. To validate the model and to establish new loss correlations, available experimental data for several transonic compressor rotors were used. Detailed loss calculation results show that the blade tip region with high Mach numbers cause shock losses that are approximately one-third of the total pressure losses. In addition, correlations are presented for total pressure-loss coefficient, profile-loss coefficient, and secondary flow-loss coefficients. These correlations allow the compressor designer to accurately estimate the blade losses and, therefore, the stage efficiency.

Nomenclature

c	=	blade cord length
D_m	=	modified diffusion factor
HR	=	immersion ratio
h	=	blade height
i	=	incidence angle
M	=	Mach number
R	=	curvature radius of the mean flow path, Fig. 4
r	=	local radius
S	=	spacing
t	=	thickness
U, V, W	=	rotational, absolute, and relative velocities
W	=	relative velocity
β	=	flow angles
γ	=	shock angle
γ_C	=	specific circulation function of a cascade
γ_R	=	specific circulation function of a rotor
δ	=	angle between the shock normal unit vector and the shock velocity vector
ζ	=	loss coefficient
θ	=	expansion angle
κ	=	specific heat ratio
σ	=	cascade solidity

Subscripts

a	=	axial direction
b,a	=	before and after the shocks in Eq. (12)
c	=	cascade, compressible
h	=	hub
s	=	shock
t	=	tip, tangential velocity component
w	=	wall
1, 2, 3	=	stations of a compressor stage

Received Dec. 23, 1995; revision received Dec. 17, 1997; accepted for publication Jan. 5, 1998.

*Professor, Turbomachinery Performance Laboratory, Department of Mechanical Engineering.

I. Introduction

THE development in the field of turbomachinery computational fluid dynamics (CFD) has reached an advanced level that allows a detailed calculation of the complex three-dimensional viscous flow through a compressor stage using Navier–Stokes codes. Case studies presented at the 1994 International Gas Turbine Institute conference displayed the capability of different CFD methods to calculate various flow quantities in detail. However, the efficiency and loss calculations revealed discrepancies between the experiment and numerical calculation. Recent experimental and numerical studies by Copenhaver et al.[1] used a multiple-blade row approach to examine the detailed flow structure inside the rotor and the stator passage. Comparison of the experimental and numerical results indicates that many features of the compressible viscous flow are captured correctly and suggests that unmeasured phenomena can be studied with some level of confidence. However, comparison of the spanwise efficiency distribution with experimental results, particularly for 100% rotor speed, shows an efficiency underprediction, from the hub up to 75% of the span, a sudden jump to overprediction ranging from 77 up to 100% of the span. This overprediction is not compatible with the physical representation of the flow. In this region, one would expect the opposite tendency, namely a decrease in efficiency as the consequence of growth of losses caused by the existence of shock, tip clearance vortices, casing boundary layer, and their mutual interactions. The study by Copenhaver et al.[1] indicates the trend of CFD application to turbomachinery final design. The preliminary design process, however, requires an accurate estimation of the compressor loss and efficiency, which can be provided by loss models that accurately represent the flow situation and are described by conservation laws.

To calculate the compressor stage efficiency accurately, the compressor designer often uses loss correlations that account for different loss mechanisms within the compressor stage flowfield. Miller and Hartmann[2] and Miller et al.[3] conducted fundamental research on transonic compressors, where they primarily investigated the shock losses. Gostelow, Smith and co-workers[4–10] focused their experimental research on single-stage, high-Mach-number axial compressors. Their comprehensive experimental research includes the performance

evaluation of several rotors. Koch and Smith[11] presented a method for calculating the design-point efficiency potential of a multistage compressor. Monsarrat et al.[12] performed similar investigations on single-stage, high-Mach-number compressor stages. Several papers have discussed experimental and theoretical shock-loss investigations. Schwenk et al.[13] considered a normal shock in the entrance region of the cascade using a Prandtl–Meyer expansion. Levine,[14] Balzer,[15] and Swan,[16] made efforts to calculate the shock losses by estimating the shock position. The proposed methods, particularly, that of Levine and Swan, found application in compressor design. Similar to Schwenk et al., the methods by Levine, Balzer, and Swan include the assumption of a normal shock. Levine and Swan considered the acceleration on the suction surface by using the continuity equation and a Prandtl–Meyer expansion; however, Balzer disregarded the expansion completely and used the continuity requirement. To construct the flowfield Levine assumes an oblique shock formed at the leading edge, which is followed by an expansion fan generated along the suction surface. Levine defines the point e on the suction surface (Fig. 1) so that the characteristic generated there is just intercepted by the leading edge of the adjacent blade at location L, and he determines the Mach M_e from the Prandtl–Meyer relation. Although Levine's work is considered as a thorough treatment of the subject, it does not address the core of the problem, namely the determination of the shock position. The deficiencies in the existing methods can be summarized as follows:

1) They cannot accurately calculate the shock position, which is a prerequisite for accurately predicting the shock losses.

2) The Mach number calculated by the Prandtl–Meyer expansion on the suction surface does not represent the shock Mach number along the channel width; Swan[16] partially corrected this deficiency by building an average Mach number.

3) The description of the physical process is not complete: The Prandtl–Meyer expansion combined with the continuity requirement is not sufficient to describe the shock mechanism inside a compressor blade channel.

In an effort to predict the loss creation in the inlet area of a compressor blade with supersonic relative inlet flow, Freeman and Cumpsty[17] applied the conservation laws to a control volume. They assumed a subsonic flow at the rear of the control volume with a uniform Mach number M_2 in the direction of the blades and applied the momentum equation in that direction. They argued that the downstream pressure p_2 acting on the entire gap in the momentum equation is equivalent to assuming that the downstream pressure acts along the blade surface from the leading edge as far as the downstream boundary to the inlet region. Freeman and Cumpsty asserted that their method is not entirely correct, but further argued that the error caused by this, which in their opinion forms a part of higher-order terms, can be neglected. Incorporating their assumptions, Freeman and Cumpsty arrived at a momentum equation that includes higher-order terms. Eliminating the pressure terms, they obtained a final equation, plotted the right-hand and the left-hand sides (LHS and RHS, respectively) of this equation, and found considerable discrepancies between the LHS and RHS. To find a solution, Freeman and Cumpsty suggested an iteration procedure to find M_2.

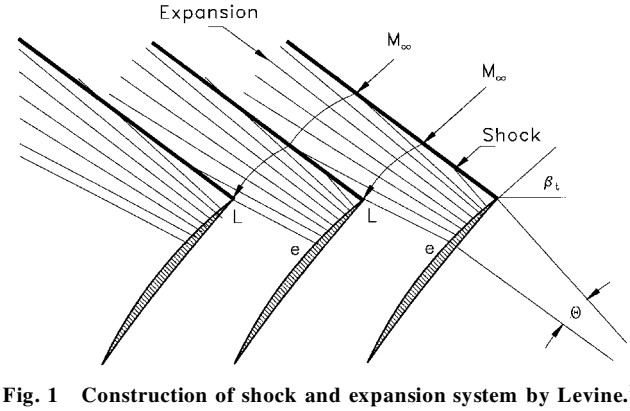

Fig. 1 Construction of shock and expansion system by Levine.[15]

The method discussed in the preceding text contains assumptions that violate the consistency of the conservation laws leading to an erroneous equation (Freeman and Cumpsty,[17] Eq. 4). These are as follows:

1) Assuming a uniform M_2 without specifying its location is an invalid assumption.

2) The assumption about the downstream pressure p_2 as described earlier is not substantiated.

3) The conservation of momentum is not correctly applied to the control volume. The component of the blade force, particularly the drag component in the blade direction is declared as the higher-order terms to be neglected. As a result, the earlier equation does not simultaneously satisfy the conservation laws. It is only valid if the blade thickness is equal to zero and the flow angle coincides with the blade angle. This case, however, exhibits the trivial solution for the normal shock of a perfect gas through a channel with constant cross section. However, M_2 and the shock position can be accurately determined as is shown in this paper.

Shock structure in transonic compressor rotors has been the subject of several experimental investigations. Prince[18] evaluates three-dimensional shock structures for transonic/supersonic compressor rotors using holography, laser velocimetry, and high-frequency pressure transducers. Prince compared the measured shock angles with those predicted by conventional cascade analysis and found discrepancies ranging from 20 to 60% resulting in shock-angle differences of 15–20 deg. Wennerstrom and Puterbaugh[19] published a three-dimensional model for the prediction of shock losses in compressor blades. They state that their model differs from a classical Miller–Lewis–Hartman (MLH) normal shock model by taking into account the spanwise obliquity of the shock surface resulting from a leading-edge sweep, blade twist, and solidity variation. They obtain the upstream shock Mach number using the MLH normal shock model. Furthermore, they assume the suction surface Mach number to be that resulting from Prandtl–Meyer expansion from the relative inlet value through an angle equal to the difference between the relative inlet flow angle and the suction surface angle at the impingement point. For the calculation of the angle of the shock surface relative to the upstream flow, Wennerstrom and Puterbaugh introduced a geometric relation that contains the stream surface slope, the blade lean angle, and the relative flow angle. Using the normal shock relations to calculate the upstream Mach number, which is then averaged, the authors integrated the procedure into an existing streamline curvature code to calculate the loss coefficients and, thus, the efficiency of three test compressors. With regard to their efficiency comparison with the MLH method and experiment, the authors found inconsistent results. In all three cases, their method predicted a higher isentropic efficiency than the MLH model did. Compared with experimental results, however, the method slightly overpredicted the first compressor efficiency, underpredicted the second compressor efficiency by 0.5%, and overpredicted the third compressor efficiency by 0.5%. The main reason for the efficiency discrepancy may be attributed to inaccurate calculation of the angle of the shock surface relative to the upstream flow. The relation introduced by Wennerstrom and Puterbaugh[19] is constructed from the normal shock assumption and the blade surface geometry to account for spanwise obliquity. Although the test calculations did not prove the validity of their shock-loss model, as the authors concluded, they did illustrate the magnitude of the reduction in shock losses and particularly the spanwise obliquity of the shock.

The deficiencies mentioned earlier motivated Schobeiri[20] to generate a comprehensive study that deals with loss mechanisms within transonic and supersonic compressors. In the following, a brief description of a new shock-loss model by Schobeiri is presented. For the development of this model, the passage shock is assumed to be an oblique shock, whose position changes according to the operating point and may include a normal shock as a special case. Furthermore, it is assumed that the blading has a sufficiently sharp leading edge, where the shocks are attached at least at the design point, with no detached bow waves expected. Furthermore, it is assumed that the compressor cascade flow under investigation can be represented by an equivalent two-dimensional steady flow, where the cascade periodicity requirement is fulfilled. Starting from these assumptions, we use the conservation laws of continuity, momentum, and energy, and a few geometric relations. At the outset, it should be mentioned that none of the existing appropriate models mentioned earlier has used the momentum equation. This equation, if applied properly, helps accurately determine the shock angle, which is one of the major parameters in shock-loss calculation.

II. Shock-Loss Model, Analytical Method

Figure 2 shows the shock situation with the inlet flow angle β_1, the metal angle β_t, and the incidence angle i, which changes during an off-design operation. To determine the shock position the continuity equation, the Prandtl–Meyer expansion, and the momentum equation are used. For the control volume in Fig. 2 the continuity requirement is

$$\rho_1 V_1 S_1 \sin\beta_1 = \rho_s V_s s_s \cos\delta (h_S/h_1) \tag{1}$$

with h_1 and h_S as the height of the stream tube at the blade leading edge and the shock-impingement point B (Figs. 2 and 3), respectively. Using the gasdynamics relationship, Eq. (1) is written as

$$\frac{h_1}{h_S}\frac{S_1 \sin\beta_1}{S_S \cos\delta} = \frac{\rho_S}{\rho_1}\frac{V_S}{V_1} = \frac{M_S}{M_1}\left\{\frac{1 + [(\kappa-1)/2]M_1^2}{1 + [(\kappa-1)/2]M_S^2}\right\}^{(1/2)[(\kappa+1)/(\kappa-1)]} \tag{2}$$

with the geometric relation

$$\delta = (\pi/2) + \beta_S - \gamma \tag{3}$$

The incidence and the expansion angle are coupled by

$$i = \theta - \nu_S + \nu_1 \tag{4}$$

where ν is determined from the Prandtl–Meyer expansion law

$$\nu = \sqrt{(\kappa+1)/(\kappa-1)}\arctan\sqrt{[(\kappa-1)/(\kappa+1)](M^2-1)} - \arctan\sqrt{M^2-1} \tag{5}$$

To complete the determining set of equations, the momentum balance is applied to the control volume shown in Fig. 2. The control volume is thought of as a portion of a stream tube, which is bound by two adjacent meridional stream surfaces shown in Fig. 3. The area on the suction surface that is directly exposed to the shock is represented by the hatched area CBB′C′. Neglecting the shear stress along the passage shock AB and the blade-wall portion BC shown in Fig. 2, the momentum equation in tangential direction is written as

$$\int_{S_1} V_1 \cos\beta_1 \, d\dot{m}_1 - \int_{S_S} V_S \cos\beta_S \, d\dot{m}_S + \int_{S_S} - p_S \cos(\beta_S - \delta)\, dS_S + \int_{S_W} - p_W \cos\alpha_W \, dS_W = 0 \tag{6}$$

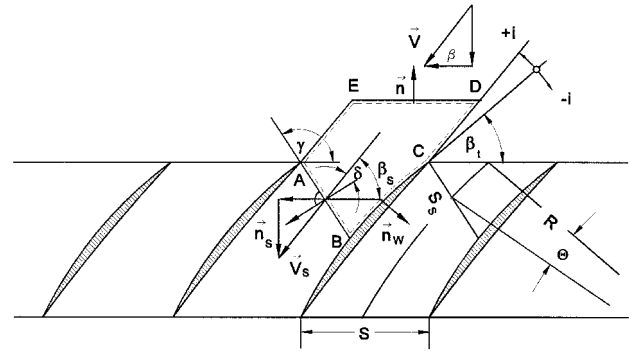

Fig. 2 Shock-wave configuration, angle definition, and normal unit vectors.

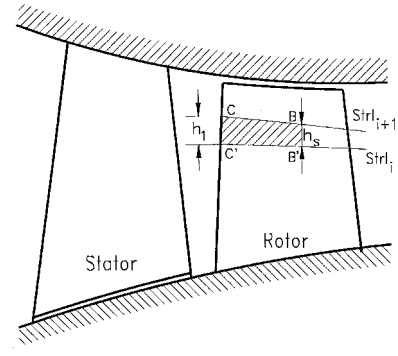

Fig. 3 Stream tube with the inlet height h_1 and the shock impingement height h_S bound by two streamlines $Strl_i$ and $Strl_{i+1}$ to explain the continuity requirement.

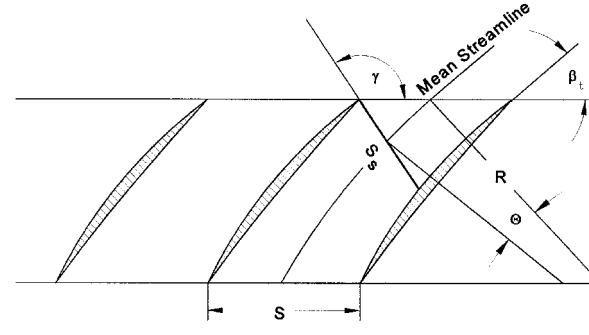

Fig. 4 Introduction of mean streamline with curvature radius.

Because of the cascade periodicity, the contributions of velocity and pressure momenta along CD and EA cancel each other. As Fig. 2 shows, because of the cascade periodicity, the pressure at point A is identical to the pressure at point C. Furthermore, point B on the suction surface represents the common endpoint for both distances AB and CB. This means that the pressure distributions along AB and CB have exactly the same beginning and ending values, but may have different distributions between points AB and CB. Assuming that the pressure integrals along the shock-front AB and the blade-contour portion CB are approximately equal, their projections in circumferential direction may cancel each other, leading to

$$\frac{V_1}{V_S} = \frac{\cos\beta_S}{\cos\beta_1} = \frac{M_1}{M_S}\left\{\frac{1 + [(\kappa-1)/2]M_S^2}{1 + [(\kappa-1)/2]M_1^2}\right\}^{1/2} \tag{7}$$

Finally, we arrive at a geometric closure condition that utilizes the mean streamline, which is assumed to be identical to the mean camber line of the blade with the radius R shown in Fig. 4

$$R[+\cos\beta_t - \cos(\beta_t + \theta)] = (S_S/2)\sin\gamma \tag{8}$$

$$R[-\sin\beta_t + \sin(\beta_t + \theta)] = (S_S/2)\cos\gamma + (S_1/2) \quad (9)$$

The shock angle γ is determined from

$$\tan\gamma = \frac{\cos\beta_t - \cos(\beta_t + \theta)}{-\sin\beta_t + \sin(\beta_t + \theta) - \frac{1}{2}(S_1/R)} \quad (10)$$

Considering the preceding procedure, the continuity equation yields

$$\frac{h_1}{h_S}\frac{\sin(\beta_t + i)\sin\gamma}{2(R/S_1)[\cos\beta_t - \cos(\beta_t + \theta)]\sin(\gamma - \beta_S)} = \frac{M_S}{M_1}\left\{\frac{1 + [(\kappa - 1)/2]M_1^2}{1 + [(\kappa - 1)/2]M_S^2}\right\}^{(1/2)[(\kappa + 1)/(\kappa - 1)]} \quad (11)$$

Equation (11) represents a general relationship between M_S and the undisturbed M_1 with R/S_1 as a cascade geometry parameter (Figs. 2–4). It is valid for axisymmetric cascades with different spacings at the inlet and exit. For a rectilinear cascade, the spacings at the inlet and exit are identical and may be set: $S_1 = S_2 = S$. With Eqs. (2–11) the shock quantities such as δ, β_s, γ, and M_s can be calculated easily. The shock loss is

$$\zeta_S = \frac{P_b - P_a}{P_b} = 1 - \left[\frac{(\kappa + 1)M_S^2\cos^2\delta}{2 + (\kappa - 1)M_S^2\cos^2\delta}\right]^{\kappa/(\kappa - 1)} \times \left[1 + \frac{2\kappa}{\kappa + 1}(M_S^2\cos^2\delta - 1)\right]^{(-1)/(\kappa - 1)} \quad (12)$$

where P_b and P_a represent the total pressure before and after the shock. As an example, for $\beta_t = 30$ deg and the incidence angle $i = 0$ deg, the preceding equation system [Eq. (12)] is used to calculate M_S, θ, γ, the total pressure ratio and, thus, the shock losses. The preceding equations represent a new model for implementation into a design code such as streamline curvature code. They also exhibit an appropriate tool for parameter studies. Equations (8–10) represent the closure condition utilizing the mean streamline for circular arc blades. For an arbitrary blade geometry, similar closure conditions can be constructed by using the specific geometry of the blade under investigation. The geometry may include multicircular arc blades or any blades, whose shape is generally arbitrary. The model discussed earlier is applicable to operation points, where the shock is attached to the leading edge. It also may be applied to operations, where the shock is slightly detached from the leading edge. In this case the method may yield acceptable results. Adverse operation regimes that provoke stall conditions, where partial or total flow separation may occur, may violate the assumptions made for establishing the theory. Therefore, the application of the theory to these cases may yield results that are not quite accurate. It should be pointed out that the author has not applied the theory to such cases.

In the following section, the results of a parameter study will be presented to show the effect of inlet Mach number on shock Mach number, expansion angle, and the shock position. Then the equations will be implemented into a compressor shock-loss calculation procedure.

III. Results: Parameter Study

The configuration of the figures in this section follows the format by Levine[14] to allow a direct comparison of both results. In this connection, it should be mentioned that the variation of S/R from 0.0 to 1.0 may not be representative for advanced transonic or supersonic compressors. The latter may have a large radius curvature resulting in small S/R ratios. The results of the preceding equations are shown in Fig. 5, where the shock Mach number is plotted as a function of S/R with M_1 as the parameter. This figure shows that by increasing the spacing ratio the shock Mach number continuously increases and approaches an asymptotic value. These results are similar to those presented by Levine.[14] However, the values are different because of the simplifying assumptions made by Levine. Keeping the inlet Mach number constant, the increase of spacing ratio leads to a higher θ, as shown in Fig. 6. This is in agreement with the observations by Miller et al.[2] They found that increasing the spacing moves the shock position farther downstream. On the other hand, increasing the inlet Mach number at a constant S/R leads to a smaller expansion angle. A similar tendency can be read from charts by Levine. For $M_1 = 1.2$ and $S/R = 0.5$, Levine's method gives $\theta = 8$ deg, whereas the method presented in this paper calculates $\theta = 9.5$ deg. As indicated previously, this difference is because of Levine's simplified assumptions. Figure 7 shows γ as a function of S/R with M_1 as the parameter. This figure exhibits the significant effect of the inlet Mach number on the shock position. For a given S/R, the γ increases with increasing the inlet Mach number. This result is fully consistent with those found in Fig. 6. For the parameter study presented in Fig. 7, shock-position angles range from 115 to 170 deg. However, as mentioned previously, the variation of S/R from 0.0 to 1.0 may not be representative of advanced transonic or supersonic compres-

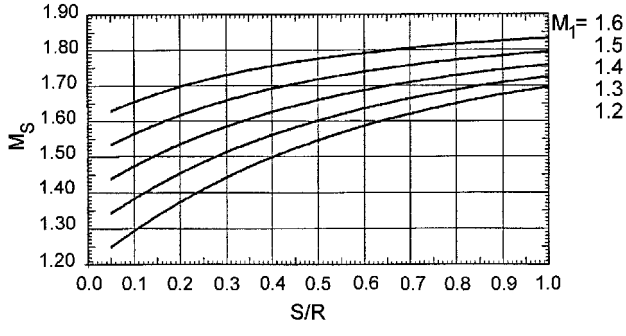

Fig. 5 Shock Mach number as a function of S/R with M_1 as a parameter with $\beta_t = 30$ deg and $i = 0$ deg.

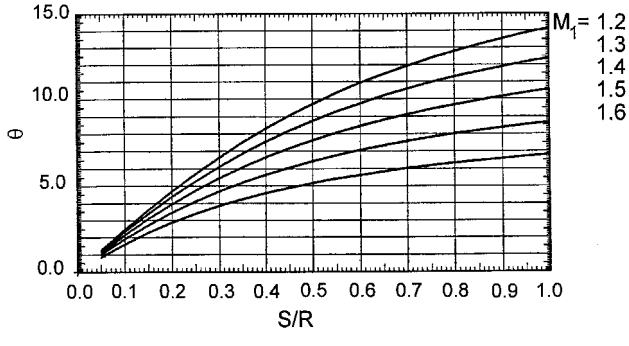

Fig. 6 θ as a function of S/R with M_1 as a parameter with $\beta_t = 30$ deg and $i = 0$ deg.

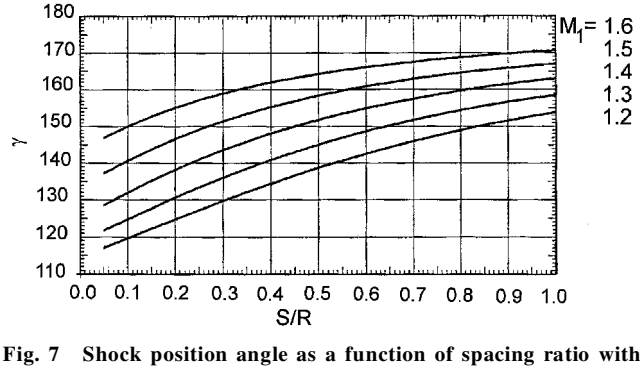

Fig. 7 Shock position angle as a function of spacing ratio with inlet Mach number as a parameter and $\beta_t = 30$ deg.

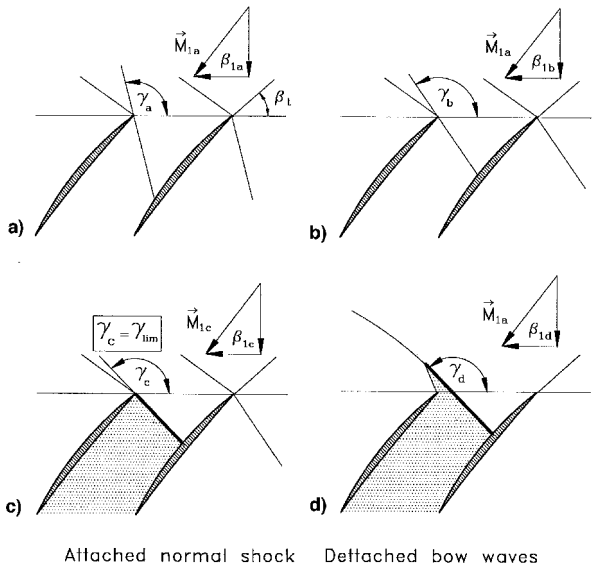

Fig. 8 Change of γ for a given cascade geometry at different operation points.

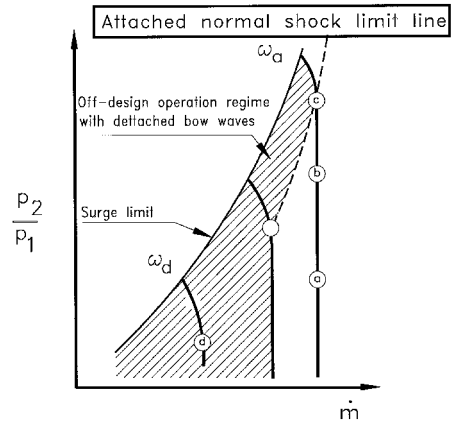

Fig. 9 Effect of γ change described in Fig. 8 on compressor performance map.

sors. The latter may have relatively small maximum thicknesses and high radii of curvature on suction and pressure surfaces resulting in small *S*/*R* ratios and, thus, different shock angles. Once the shock angle is calculated at the design point, it may undergo changes during an off-design operation. The off-design operation may place a limitation on the shock-angle range as Fig. 8 illustrates. Beginning with a design-point speed line the operating point (Fig. 8a) is given by M_1 with a uniquely allocated β_1 that satisfies the unique incidence criterion. Increasing the back pressure from the design-point backpressure to a higher level (Fig. 8b) causes the passage shock to move toward the cascade entrance. By further increasing the back pressure from Fig. 8b to 8c a normal shock is established, which is still attached. The corresponding γ can be set equal to $\gamma_{lim} \equiv \gamma_{at}$. Decreasing the mass flow beyond this point causes the shock to detach from the leading edge as shown in Fig. 8d. Reducing the rotational speed changes the incidence and may lead to further moving the shock from the leading edge as shown in Fig. 8d. These operating points are plotted schematically in a compressor performance map shown in Fig. 9 with a surge limit and an attached normal shock line.

IV. Results: Pressure Losses in an Axial Flow Compressor Stage

To calculate the shock losses in a transonic or a supersonic axial flow compressor, the shock model developed in Sec. II

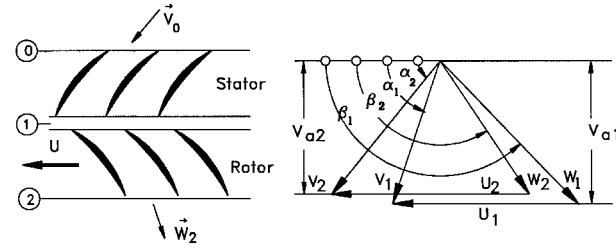

Fig. 10 Compressor-stage velocity triangles, vectors, and angle definitions used in diffusion factor relation.

is integrated into a loss-calculation procedure. To quantitatively describe the loss coefficient, the compressor designer usually utilizes the flow deflection represented by the diffusion factor as a variable and the spanwise immersion as a parameter. In this section we follow the compressor designer nomenclature and present the results as a function of the diffusion factor in the spanwise direction. The following diffusion factor has been accepted and widely used by compressor aerodynamicists:

$$D = 1 - \frac{W_2}{W_1} + \frac{1}{\sigma}\frac{r_2 V_{t2} - r_1 V_{t1}}{(r_1 + r_2) W_1} \tag{13}$$

It includes the effect of the rotation in its third term. Using the angle definition in Fig. 10 and the dimensionless parameters

$$\phi = \frac{V_{a2}}{U_2}, \qquad \chi = \frac{U_1}{U_2} = \frac{r_1}{r_2}$$
$$\mu = \frac{V_{a1}}{V_{a2}} = \frac{W_{a1}}{W_{a2}} \tag{14}$$

the rearrangement of Eq. (13) results in

$$D = 1 - \frac{1}{\mu}\frac{\sin\beta_1}{\sin\beta_2} + \frac{\chi \sin\beta_1}{\sigma(\chi + 1)} \times \left[\frac{1}{\mu\chi\phi}(1 - \chi^2) + \cot\beta_1 - \frac{1}{\mu\chi}\cot\beta_2\right] \tag{15}$$

The expression in the parentheses exhibits the blade-specific circulation, where the density change is not considered. To account for the change of density, Schobeiri[20] modified the diffusion factor by introducing the compressibility effect that is briefly summarized. To consider the effect of compressibility on the maximum velocity ratio and thus on the diffusion factor, Schobeiri introduced the specific circulation function for linear and annular cascades, and compressor stages. For better understanding, this is started with the the simplest case, namely a linear cascade, by introducing the inlet density ρ_1

$$\gamma_{C_c} = \frac{A_c}{\rho_1 V_\infty V_{a1}^S} = \frac{\rho_\infty}{\rho_1}(V_{t1} - V_{t2})\frac{1}{V_{a1}} \tag{16}$$

The first subscript *C* refers to cascade second and the second one to compressible flow. The freestream density ρ_∞ can be expressed in terms of the density at the inlet and a finite increase $\rho_\infty = \rho_1 + \Delta\rho$. Outside the boundary layer a potential flow is assumed that is not influenced by small perturbations. With this assumption, the Euler equation combined with the speed of sound may be applied

$$V\,dV = -C^2\frac{d\rho}{\rho} \tag{17}$$

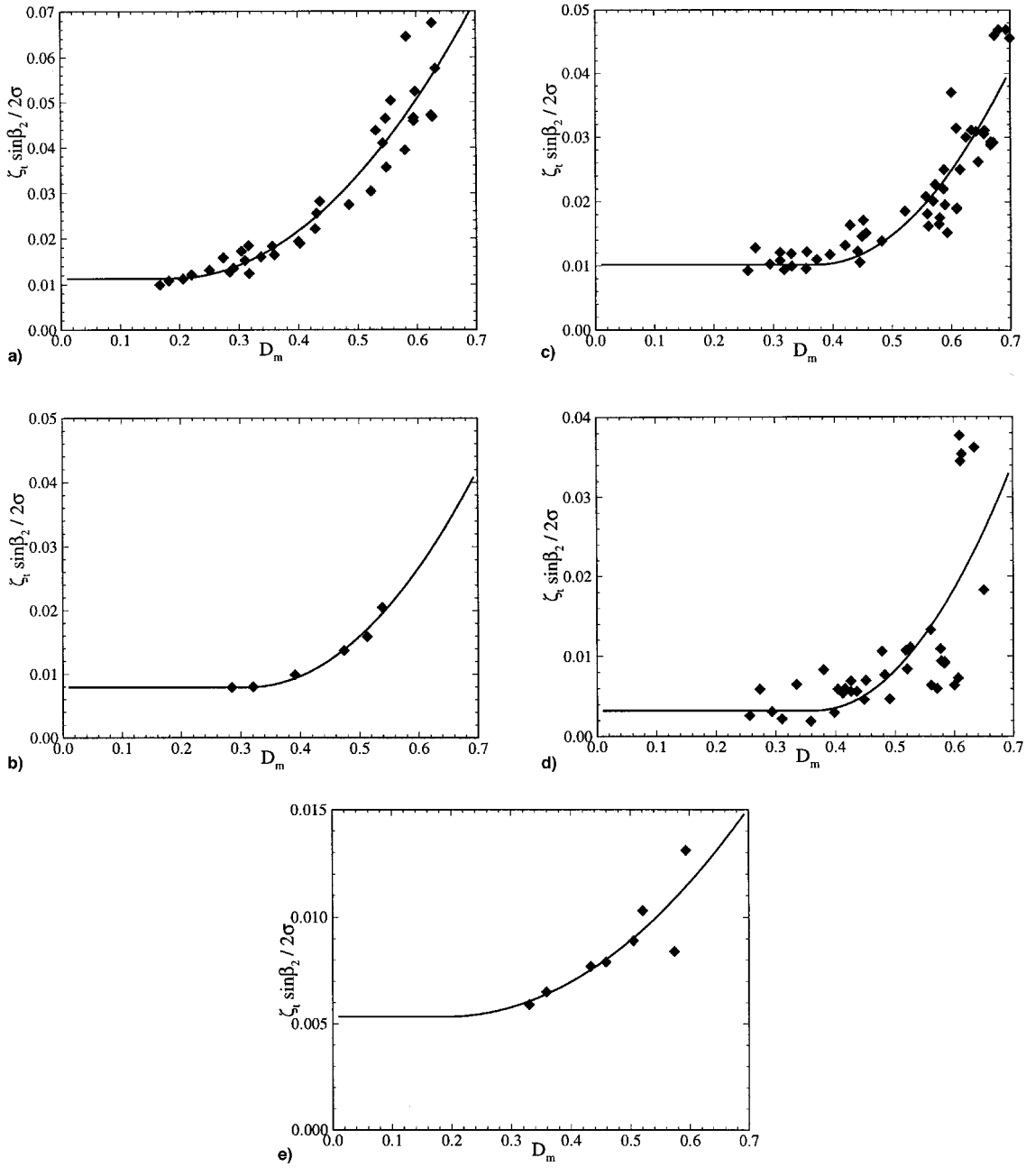

Fig. 11 Total-loss parameter for HR = a) 0.1, b) 0.3, c) 0.5, d) 0.7, and e) 0.9. Rotor data from GE-1B, 2B, and 2D.

with C as the speed of sound. For small changes, the flow quantities can be related to the quantities at the inlet

$$V = V_1 + \Delta V, \qquad C = C_1 + \Delta C$$
$$\rho = \rho_1 + \Delta\rho, \qquad d\rho \cong \Delta\rho \tag{18}$$

The preceding relations are introduced into Eq. (17) and the differentials are approximated by differences and the higher-order terms are neglected. After some rearranging the density changes are obtained by

$$\frac{\Delta\rho}{\rho_1} = -M_1^2 \left(\frac{V_2}{V_1}\right)\left(\frac{V_2}{V_1} - 1\right) \tag{19}$$

Introducing Eq. (19) into the relation $\rho_\infty = \rho_1 + \Delta\rho$ results in

$$\frac{\rho_\infty}{\rho_1} = \left[1 - M_1^2 \left(\frac{\sin\beta_1}{\sin\beta_2}\right)\left(\frac{\sin\beta_1}{\sin\beta_2} - 1\right)\right] \tag{20}$$

Implementing Eq. (20) into Eq. (16) obtains the specific circulation functions for linear cascade and stators with cylindrical streamlines:

$$\gamma_{C_c} = \left[1 - M_1^2 \left(\frac{\sin\beta_1}{\sin\beta_2}\right)\left(\frac{\sin\beta_1}{\sin\beta_2} - 1\right)\right](\cot\beta_1 - \cot\beta_2) \tag{21}$$

The expression in the preceding bracket reflects the Mach number effect on the specific circulation function. Using the same principle, the generalized circulation function for the rotor is obtained by

$$\gamma_{R_c} = \left[1 - M_1^2 \left(\frac{\sin\beta_1}{\sin\beta_2}\frac{1}{\mu}\right)\left(\frac{\sin\beta_1}{\sin\beta_2}\frac{1}{\mu} - 1\right)\right] \times \left[\frac{1}{\mu\chi\phi}(1 - \chi^2) + \cot\beta_1 - \frac{1}{\mu\chi}\cot\beta_2\right] \tag{22}$$

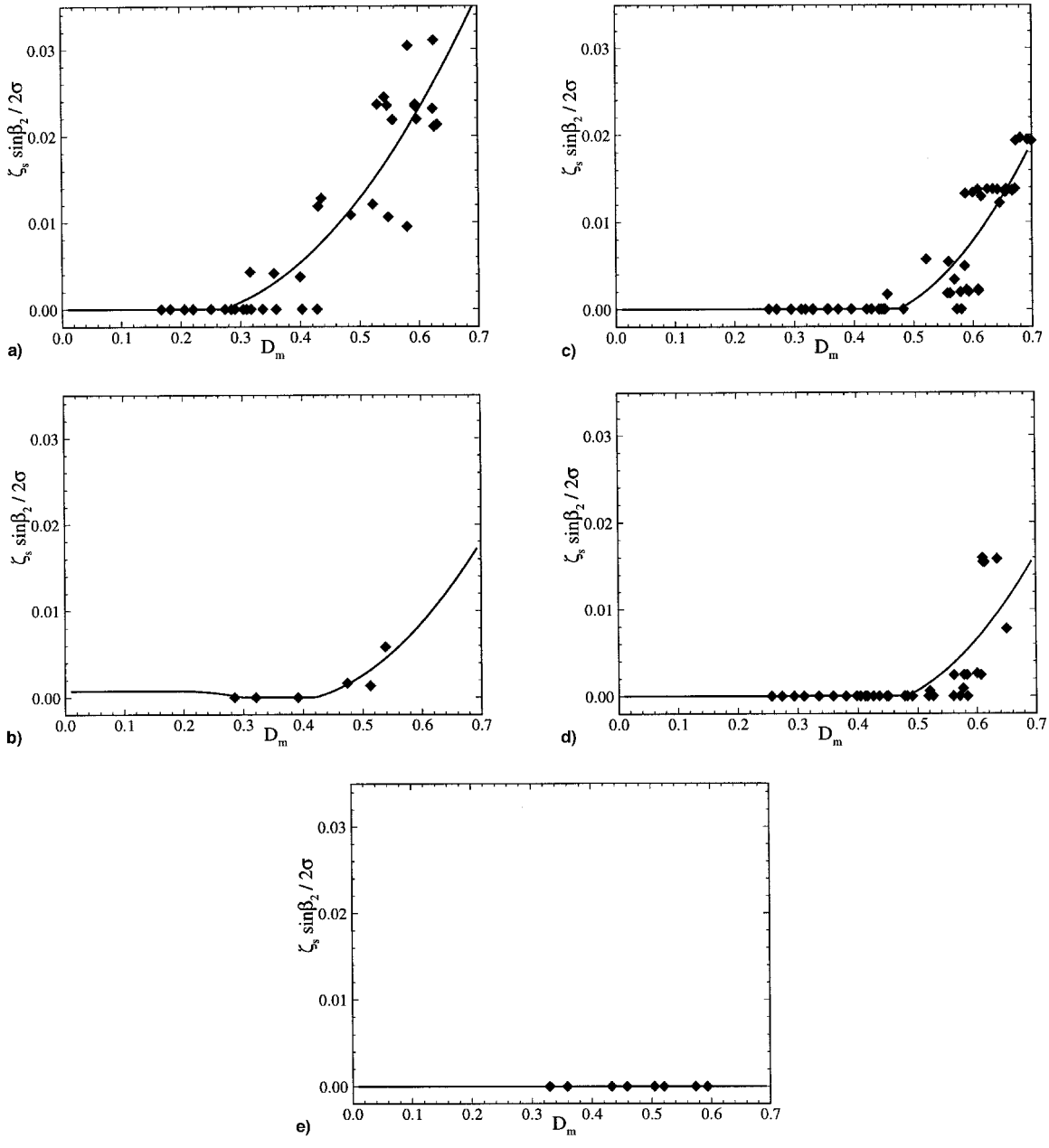

Fig. 12 Shock-loss parameter for HR = a) 0.1, b) 0.3, c) 0.5, d) 0.7, and e) 0.9. Rotor data from GE-1B, 2B, and 2D.

This equation allows calculation of the specific circulation function that accounts for the compressibility effects. Introducing Eq. (22) into Eq. (15) results in a modified version of Eq. (15), which was introduced by Schobeiri[20]

$$D_m = 1 - \frac{1}{\mu}\frac{\sin\beta_1}{\sin\beta_2} + \frac{\chi \sin\beta_1}{\sigma(\chi+1)}\left[\frac{1}{\mu\chi\phi}(1-\chi^2) + \cot\beta_1 - \frac{1}{\mu\chi}\cot\beta_2\right]\left[1 - \frac{1}{\mu}\frac{\sin\beta_1}{\sin\beta_2}M_1^2\left(\frac{1}{\mu}\frac{\sin\beta_1}{\sin\beta_2} - 1\right)\right] \quad (23)$$

In the following, this diffusion factor is used to establish correlations for the individual losses as well as the total losses. For this purpose the shock-loss model was rearranged so that it was expressed in terms of modified diffusion factor with the immersion ratio $HR = (r - r_h)/(r - r_t)$ as the parameter. The total pressure losses encountered in an axial compressor stage are as follows:

1) The blade primary losses generated by the wall shear stress: The primary losses are restricted to the middle of the blade surface area and are not affected by the secondary vortices generated by the secondary flow on the blade hub and tip.

2) The trailing-edge mixing losses are a result of the thickness of the trailing edge that causes a wake defect, mixing, and additional entropy increase. From an experimental point of view these two losses are not separable because the total pressure measurements occur at a certain distance downstream of the trailing-edge plane and inherently include the wake's total pressure defect. Frequently, the combination of these two losses is called profile loss.

3) Shock losses are encountered in compressor stages with subsonic absolute and high transonic to supersonic relative inlet flow conditions. Based on an angle incidence and the shock position, these losses may generate considerable entropy increases, resulting in a significant deterioration of the stage efficiency. The shock losses are approximately of the same order of magnitude as the profile losses.

4) Secondary losses that are a result of the end-wall boundary-layer development, blade-casing clearance, and tip vortices.

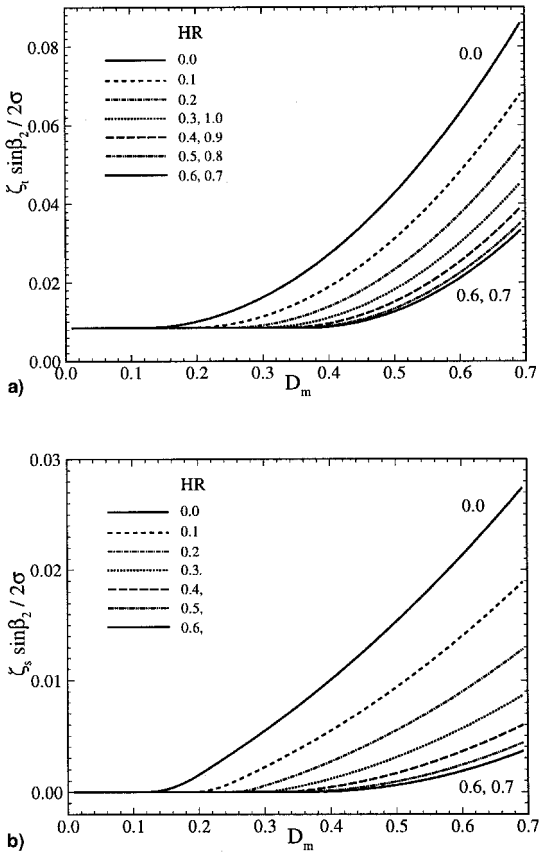

Fig. 13 a) Total-loss parameter and b) shock-loss parameter as a function of modified diffusion factor.

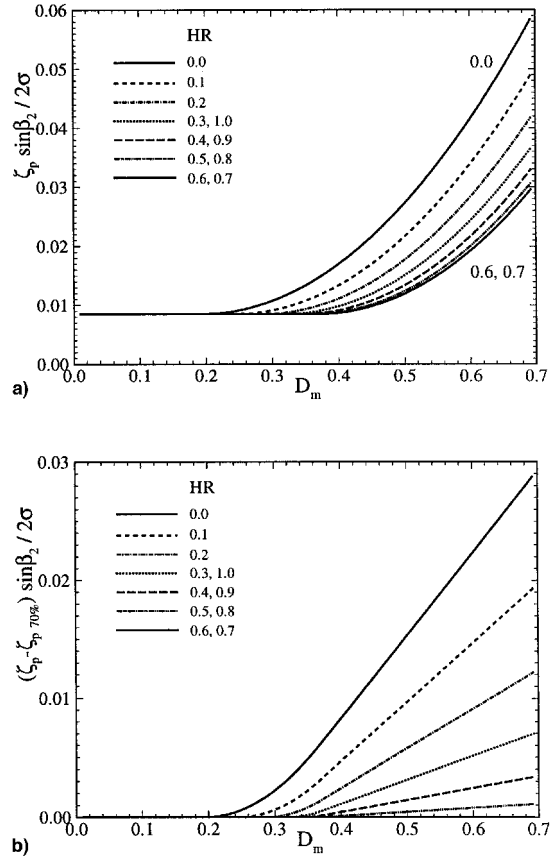

Fig. 14 a) Profile-loss parameter and b) difference in profile-loss parameter with respect to minimum profile-loss parameter as a function of modified diffusion factor.

5) Secondary flow losses as a result of compressor blades with shrouds: A comprehensive treatment of losses is found in a study by Schobeiri.[20]

To establish a set of correlations that accounts for different compressor loss mechanisms, the existing publicly available experimental data were re-evaluated, particularly those by Gostelow and Krabacher[8] and Krabacher and Gostelow[9,10] who used four single-stage compressors with multi-circular-arc profiles. A detailed description of the compressor facility and the stages are found in the reports by Gostelow and Krabacher[8] and Krabacher and Gostelow.[9,10] The data analysis used the following information: 1) The total pressure losses as a function of the diffusion factor in the spanwise direction; 2) inlet, exit, and incidence angles; 3) Mach numbers; 4) velocities; and 5) geometry. To consider compressibility effects, the modified diffusion factor in Eq. (23) was used with the information from Gostelow and Krabacher[8] and Krabacher and Gostelow.[9,10] Correlations were derived for total-loss coefficients, profile-loss coefficients, and secondary flow-loss coefficients from the experimental data. To obtain a correlation for the profile-loss coefficient, the shock-loss coefficients consistent with the total-loss coefficient defined in the reports by Gostelow and Krabacher[8] and Krabacher and Gostelow[9,10] are calculated and subtracted from the total-loss coefficients. By definition, this so-called profile-loss coefficient not only includes the primary losses but also contains the losses resulting from the secondary flow. Figures 11a–11e show the total pressure-loss parameter as a function of the modified diffusion factor for the immersion ratios *HR* from 0.1 to 0.9 as a parameter. The symbols represent the measurements for three different compressor rotors, GE-1B, GE-2B, and GE-2D. The highest loss parameter is encountered near the tip, where the shock losses and secondary flow-losses are present. Using the information from Gostelow and Krabacher[8] and Krabacher and Gostelow[9,10] for the same immersion ratios from 0.1 to 0.9, shock-loss coefficients are calculated and plotted in Figs. 12a–12e. As expected, the highest shock loss occurs at the tip because of the high-tip Mach number. For the diffusion factor ranging from D_m = 0.1 to 0.3, Mach-number effects are not noticeable. At the tip region with *HR* = 0.1 and 100% rpm (Fig. 12a), the shock losses contribute to about 40% of the total losses. This order of magnitude emphasizes the importance for accurately predicting the shock losses in context of overall total loss and efficiency prediction. Figure 12e exhibits an overall zero shock-loss coefficient at the hub, indicating the absence of shock at the hub at any rpm.

The diagrams in Figs. 11a–11e are summarized in Fig. 13a, where all of the data are statistically evaluated. Figure 13a exhibits the total pressure-loss parameter as a function of the modified diffusion factor with the immersion ratio as parameter. Highest total pressure loss occurs at the casing with *HR* = 0, where the shock and boundary interaction determines the loss parameter. The losses continuously decrease by moving toward the blade midsection up to *HR* = 0.6. The total pressure-loss coefficient assumes a minimum at *H* = 0.7. At this radius, the secondary-flow effect apparently diminishes completely, so that the total pressure-loss coefficient corresponds to the primary-loss coefficient. For immersion ratios greater than *H* = 0.7, the losses start increasing again, which indicates the strong effect of the secondary flow. Figure 13b summarizes the shock-loss situation from tip to hub (*HR* = 0–1.0). Highest shock losses occur at the tip region and decrease toward the hub, as seen in previous shock figures. As previously mentioned, subtracting the shock-loss coefficients from the total-loss coefficients provides profile-loss coefficients. The resulting profile-loss coefficients plotted in Fig. 14a are approximately 30% smaller than the total pressure-loss coefficient shown in Fig. 13a. The fact that the total pressure-loss coefficients exhibit a minimum at *H* = 0.7, where the second-

ary flow-effect diminishes, enables the compressor designer to estimate the secondary flow losses. To determine the distribution of the secondary flow losses, one can start from the profile-loss distributions at different spanwise locations and subtract the losses at $H = 0.7$. As a result, these losses include the effect of the secondary flows associated with wall boundary-layer development and clearance vortices. Figure 14b shows the distribution of the secondary loss parameter as a function of the modified diffusion factor and exhibits a linear dependency of the secondary loss parameter as a function of the modified diffusion factor with the immersion ratio as a parameter. Because the diffusion factor is directly related to the lift force and, thus, to the lift coefficient ($C_L c/s$) as a linear function, one may conclude that the secondary flow losses are linearly proportional to ($C_l c/s$). This is in agreement with the measurements by Grieb et al.[21] and in contrast to the correlation proposed earlier by Carter[22] that includes the term $(C_L c/s)^2$ and is adopted by many other researchers.

V. Concluding Remarks

In this paper a new shock-loss model was presented that overcomes the weakness of the existing loss models. It accurately calculates the expansion angle, the shock position, and the shock losses. Existing published data were then re-evaluated and detailed correlations were presented. Correlations were established for the total pressure-loss coefficient, profile-loss coefficients, and the secondary flow-loss coefficients. These correlations allow the compressor designer to accurately estimate the blade losses and, therefore, the stage efficiency. The integration of this new shock-loss model into a design code, such as a streamline curvature code, exhibits a simple and practical tool to accurately calculate shock loss.

References

[1]Copenhaver, W. W., Hah, C., Puterbaugh, S. L., "Three-Dimensional Flow Phenomena in a Transonic, High Through Flow, Axial-Flow Compressor Stage," *Journal of Turbomachinery*, Vol. 115, April 1993, pp. 240–248.

[2]Miller, G. R., and Hartmann, M. J., "Experimental Shock Configuration and Shock Losses in a Transonic Compressor Rotor at Design Point," NACA RM E58A14b, June 1958.

[3]Miller, G. R., Lewis, G. W., and Hartmann, M. J., "Shock Losses in Transonic Compressor Blade Rows," *Journal of Engineering and Power*, Vol. 83, July 1961, pp. 235–241.

[4]Gostelow, J. P., Krabacher, K. W., and Smith, L. H., "Performance Comparisons of the High Mach Number Compressor Rotor Blading," NASA CR-1256, Dec. 1968.

[5]Gostelow, J. P., "Design Performance Evaluation of Four Transonic Compressor Rotors," *Journal of Engineering and Power*, Vol. 93, Jan. 1971, pp. 33–41.

[6]Seylor, D. R., and Smith, L. H., "Single Stage Experimental Evaluation of High Mach Number Compressor Rotor Blading, Part I, Design of Rotor Blading," NASA CR-54581, GE R66fpd321P, April 1967.

[7]Seylor, D. R., and Gostelow, J. P., "Single Stage Experimental Evaluation of High Mach Number Compressor Rotor Blading, Part II, Performance of Rotor 1B," NASA CR-54582, GE tR67fpd236, Sept. 1967.

[8]Gostelow, J. P., and Krabacher, K. W., "Single Stage Experimental Evaluation of High Mach Number Compressor Rotor Blading, Part III, Performance of Rotor 2E," NASA CR-54583, 1967.

[9]Krabacher, K. W., and Gostelow, J. P., "Single Stage Experimental Evaluation of High Mach Number Compressor Rotor Blading, Part IV, Performance of Rotor 2D," NASA CR-54584, 1967.

[10]Krabacher, K. W., and Gostelow, J. P., "Single Stage Experimental Evaluation of High Mach Number Compressor Rotor Blading, Part V, Performance of Rotor 2B," NASA CR-54585, 1967.

[11]Koch, C. C., and Smith L. H., "Loss Sources and Magnitudes in Axial-Flow Compressors," *Journal of Engineering for Power*, Vol. 98, Jan. 1976, pp. 411–424.

[12]Monsarrat, N. T., Keenan, M. J., and Tramm, P. C., "Design Report, Single Stage Evaluation of High Mach Number Compressor Stages," NASA CR-72562 PWA-3546, July 1972.

[13]Schwenk, F. C., Lewis, G. W., and Hartman, M. J., "A Preliminary Analysis of the Magnitude of Shock Losses in Transonic Compressors," NACA RM 57A30, March 1957.

[14]Levine, P., "Two-Dimensional Inlet Conditions for a Supersonic Compressor with Curved Blades, *Journal of Applied Mechanics*, Vol. 24, No. 2, 1957, pp. 165–169.

[15]Balzer, R. L., "A Method for Predicting Compressor Cascade Total Pressure Losses when the Inlet Relative Mach Number is Greater than Unity," American Society of Mechanical Engineers, Paper 70-GT-57, June 1970.

[16]Swan, W. C., "A Practical Method of Predicting Transonic Compressor Performance," *Journal of Engineering and Power*, Vol. 83, July 1961, pp. 322–330.

[17]Freeman, C., and Cumpsty, N. A., "Method for the Prediction of Supersonic Compressor Blade Performance," *Journal of Propulsion and Power*, Vol. 8, No. 1, 1992, pp. 199–208.

[18]Prince, D. C., "Three-Dimensional Shock Structure for Transonic/Supersonic Compressor Rotors," *Journal of Aircraft*, Vol. 17. No. 1, 1980, pp. 29–37.

[19]Wennerstrom, A. J., and Puterbaugh, S. L., "A Three-Dimensional Model for the Prediction of Shock Losses in Compressor Blade Rows," *Journal of Turbomachinery*, Vol. 106, April 1984, pp. 295–299.

[20]Schobeiri, M. T., "Verlustkorrelationen für Transsonische Kompressoren," *BBC-Studies*, TR-78/20, April 1987.

[21]Grieb, H., Schill, G., and Gumucio, R., "A Semi-Empirical Method for the Determination of Multi-Stage Axial Compressor Efficiency," American Society of Mechanical Engineers, Paper 75-GT-11, 1975.

[22]Carter, A. D. S., "Three-Dimensional Flow Theories for Axial Compressors and Turbines," *Proceedings of the Institution of Mechanical Engineers*, Vol. 159, 1948, pp. 255–268.